Color constancy from blackbody illumination

Rei Kawakami,* Jun Takamatsu, and Katsushi Ikeuchi

Graduate School of Information Science and Technology, The University of Tokyo, 4-6-1 Komaba, Meguro-ku, Tokyo 153-8505, Japan

**Corresponding author: rei@cvl.iis.u-tokyo.ac.jp*

Received August 2, 2006; revised November 28, 2006; accepted January 2, 2007; posted February 7, 2007 (Doc. ID 73358); published June 13, 2007

We present a theoretical analysis of what we believe to be a new color constancy method that inputs two chromaticities of an identical surface taken under two blackbody illuminations. By using the Planck formula for modeling spectra of outdoor illumination and by assuming that a narrowband camera sensitivity function is sufficiently narrow, surface colors can be estimated mathematically. Experiments with simulation and real data have been conducted to evaluate the effectiveness of the method. The results showed that although this method is a perfect vehicle for simulation data, it produces significant errors with real data. A thorough investigation of the cause of errors indicates how important the assumptions on both blackbody illuminations and narrowband camera sensitivities are to the method. Finally, we discuss the robustness of our method and the limitation of solving color constancy using the illumination constraint.

OCIS codes: 150.0150, 150.2950.

1. INTRODUCTION

Acquiring an object's inherent color is important when modeling a real-world object. Since color appearance is significantly influenced by the illumination color, a method to remove the latter and to estimate the actual color of the object's surface, its "color constancy" in computer vision, is required. ("Color constancy" often implies recovering an object's actual surface color in the field of computer vision. Note that, to be precise, it is a psychological term meaning the ability to perceive a color as constant under varying illumination.) In general, surface-color estimation is achieved by capturing the object's color under a known illuminant and dividing it by the illumination color. We cannot, however, apply this method when the target objects are huge and are located outdoors, because the illumination condition is neither controllable nor known. It would be of great benefit to achieve color constancy only from colors received by sensors.

A number of color constancy methods have been proposed by researchers [1–13]. We can categorize them into two groups: dichromatic-based methods and diffuse-based methods. Dichromatic-based methods [1–7] require the presence of highlighting, while diffuse-based methods [8–13] require only body reflection. Since our primary objects are outdoor objects, and they have mainly body-reflection components, this paper focuses on diffuse-based methods.

Most diffuse-based methods use a single input image of objects lit by a uniformly colored illumination. Usually these methods require strong constraints in the surface-color domain, such as a prior surface-color database, and cannot accurately handle images with few surface colors [11]. Alternatively, methods based on a varying illumination color were introduced by a few researchers [14–17]. They found that the change of illumination can be a key to solving the color constancy problem. D'Zmura [14] proposed a method using approximated linear basis functions to form a closed-form equation. One drawback of the method is that it fails to provide robust estimations for real images. Ohta *et al.* [15] stabilized the estimation based on D'Zmura's assumption and the CIE daylight constraint. Finlayson *et al.* [16] used a single surface color illuminated by two different illumination colors and performed the estimation by assuming that the illumination colors form a line in an inverse-chromaticity space. Although the method is simple and elegant, the estimation tends to be unstable because of noise and outliers. Barnard *et al.* [17] utilized the Retinex algorithm [18] to automatically obtain a surface color with different illumination colors and then applied the method of Finlayson *et al.* [16] to estimate varying illumination colors in a scene.

This paper proposes a new method for color constancy that inputs two colors taken under different illumination and estimates each illumination color numerically by regarding the blackbody radiation as the illumination spectra. Blackbody radiation accurately models the light from heated metals. Moreover, several researchers reported that it can predict the general shape of daylight illuminations [6,19]. Therefore, blackbody radiation can be a better illumination model than the straight-line model used in the previous methods [16,17]. In addition to the blackbody illumination assumption, our method assumes that the sensitivity of narrowband camera sensors is sufficiently narrow [16,17,20]. The method uses three sensor values at each wavelength. This is because it was designed to use image values. However, any wavelength can be chosen for the algorithm, which means that the algorithm can be applied to a spectral separation method without any loss of generality.

The rest of the paper is organized as follows: In Section 2, we describe a problem definition of color constancy and a mathematical expression of illumination colors using blackbody radiation. In Section 3, we describe the method to estimate illumination colors. We provide simulations,

experiments, and results in Section 4. Since the results with real data included significant errors, we explore the cause of those errors with additional experiments. In Section 5, we discuss the robustness of our method, compare the blackbody model with other illumination models, and discuss the limitation of solving color constancy using illumination constraint. Finally, in Section 6, we conclude our paper.

2. THEORETICAL BACKGROUND

A. Color Constancy

Colors perceived by humans or camera sensors are light intensities that are emitted from a light source, reflected by an object surface, and filtered by color sensors. Color constancy is an inverse process of these; i.e., we estimate surface and illumination properties from a filtered color. This paper defines color constancy as the separation of an image's chromaticity i_c into surface and illumination chromaticities s_c and e_c, using the following equation:

$$i_c = s_c e_c, \quad c = \{r,g\}. \tag{1}$$

Chromaticity is defined as a ratio of the R and G values to the B value:

$$i_r = I_R/I_B, \quad i_g = I_G/I_B. \tag{2}$$

Equation (1) holds by using this definition. We use the notation r,g for chromaticities and R,G,B for intensities to distinguish them simply.

Equation (1) is derived by assuming a narrowband camera model and converting intensities into chromaticities defined by Eq. (2). Details are as follows: Image intensities of diffuse objects taken by a digital color camera can be described as Eq. (3):

$$I_c = \tau \int_\Omega S(\lambda)E(\lambda)q_c(\lambda)\mathrm{d}\lambda, \quad c = \{R,G,B\}, \tag{3}$$

$$\simeq \tau S_c E_c, \quad (S_c = S(\lambda_c), E_c = E(\lambda_c)), \tag{4}$$

where $S(\lambda)$ is the surface spectral reflectance; $E(\lambda)$ is the illumination spectral power distribution; and $q_c(\lambda)$ is the color sensor sensitivity, where index c stands for the type of sensors (R,G, and B). The integration is done over the visible spectrum (Ω), and τ is the gain determined by the aperture, the integration time, and the electronic amplification.

Next we introduce a narrowband camera model, which assumes that each color sensor has all its sensitivity concentrated on a single wavelength λ_c. That is, each sensitivity is approximated by a Dirac delta function $\delta(.)$ whose center wavelength is λ_c. Therefore, $q_c(\lambda) \simeq \delta(\lambda - \lambda_c)$, and we can subsequently obtain Eq. (4). Here $\lambda_R,\lambda_G,\lambda_B$ are the wavelengths on which the sensitivities are concentrated.

Color constancy focuses on recovering chromaticities instead of intensities. This is because there is a scale ambiguity between the surface spectral reflectance and the illumination spectral power distribution. We cannot distinguish a dark surface with bright illumination from a bright surface with dark illumination. Therefore, we convert the intensity space to the chromaticity space by substituting Eq. (4) into Eq. (2). Thus, we obtain Eq. (1). The surface chromaticity $[S_R/S_B, S_G/S_B]^t$ is rewritten as $[s_r, s_g]^t$, and the same is true for the illumination chromaticity.

B. Illumination Chromaticity

This paper assumes that most illumination spectra can be approximated by blackbody radiation. Blackbody radiation models not only the spectrum of sunlight, or of light emitted from metals heated to high temperatures, but also that of common daylight, as several researchers have reported [6,19]. The assumption is useful since an illumination chromaticity, which is a two-dimensional vector, becomes a function of a single scalar, temperature T. The scalar T is often called color temperature for representing color.

Using the blackbody assumption, an illumination chromaticity can be expressed as

$$e_r(T) = \frac{M(\lambda_R,T)}{M(\lambda_B,T)}, \quad e_g(T) = \frac{M(\lambda_G,T)}{M(\lambda_B,T)}, \tag{5}$$

where $\vec{e} = [e_r(T), e_g(T)]^t$ is the illumination chromaticity; $M(\lambda_*,T)$ is the spectral power of the blackbody radiation; T is temperature in kelvin; and $\lambda_R,\lambda_G,\lambda_B$ are the center wavelengths of the camera sensitivity. The narrowband assumption and the chromaticity definition of Eq. (2) are used to derive the last equation.

From the Planck formula, $M(\lambda,T)$ is

$$M(\lambda,T) = c_1 \lambda^{-5}[\exp(c_2/\lambda T) - 1]^{-1}, \tag{6}$$

where c_1 is 3.7418×10^{-16} (in Wm^2), c_2 is 1.4388×10^{-2} (in mK), and λ is the wavelength (in m). Substituting Eq. (6) into Eq. (5), we obtain

$$e_r(T') = k_r \frac{\Phi_B(T')}{\Phi_R(T')} \quad \left(k_r = \frac{\lambda_B^5}{\lambda_R^5}\right), \tag{7}$$

$$e_g(T') = k_g \frac{\Phi_B(T')}{\Phi_G(T')} \quad \left(k_g = \frac{\lambda_B^5}{\lambda_G^5}\right), \tag{8}$$

where $T' = c_2/T$ and $\Phi_*(T')$ are defined as follows for simplicity:

$$\Phi_R(T') = \exp(T'/\lambda_R) - 1,$$

$$\Phi_G(T') = \exp(T'/\lambda_G) - 1,$$

$$\Phi_B(T') = \exp(T'/\lambda_B) - 1. \tag{9}$$

3. OUR APPROACH

A. Problem Statement

The difference between our approach and conventional approaches is that we use the exact blackbody radiation for the model of illumination colors. Consequently, the color constancy problem becomes equivalent to estimating a color temperature T. Equation (1) shows the interdependency between surface and illumination chromaticities. Also, illumination chromaticity can be parameterized by the color temperature T, as Eqs. (7) and (8) show.

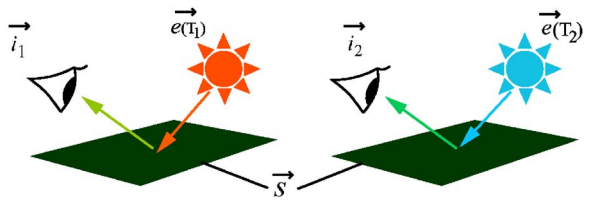

Fig. 1. (Color online) Problem statement. We estimate color temperatures from image chromaticities taken under two blackbody illuminations.

Thus, when the color temperature T is known, the illumination chromaticity and then the surface chromaticity can be calculated explicitly.

The equations to solve can be established as follows: When we observe a surface chromaticity $\vec{s}$ under two blackbody illuminations $\vec{e}(T_1)$ and $\vec{e}(T_2)$, we can estimate each color temperature T_1 and T_2 from obtained colors $\vec{i}_1$ and $\vec{i}_2$. Figure 1 illustrates those notations. Let the two image chromaticities be $\vec{i}_1=[i_{r1},i_{g1}]^t$ and $\vec{i}_2=[i_{r2},i_{g2}]^t$. We can derive the following equations, since the image chromaticities divided by their illumination chromaticities are identical to the surface chromaticity:

$$\Theta_r(T_1',T_2') = i_{r1}\Phi_R(T_1')\Phi_B(T_2') - i_{r2}\Phi_R(T_2')\Phi_B(T_1') = 0, \tag{10}$$

$$\Theta_g(T_1',T_2') = i_{g1}\Phi_G(T_1')\Phi_B(T_2') - i_{g2}\Phi_G(T_2')\Phi_B(T_1') = 0. \tag{11}$$

Color constancy will be solved if T_1' and T_2' are specified from those equations.

Detailed derivations of Eqs. (10) and (11) are as follows: The image chromaticities divided by their illumination chromaticities are identical to the surface chromaticity, as Eq. (1) shows. Therefore, the following equations can be derived:

$$i_{r1}/e_{r1} - i_{r2}/e_{r2} = 0, \tag{12}$$

$$i_{g1}/e_{g1} - i_{g2}/e_{g2} = 0, \tag{13}$$

while Eqs. (7) and (8) can be converted as follows:

$$1/e_r = \Phi_R(T')/k_r\Phi_B(T'), \tag{14}$$

$$1/e_g = \Phi_G(T')/k_g\Phi_B(T'). \tag{15}$$

By substituting Eqs. (14) and (15) into Eqs. (12) and (13), Eqs. (10) and (11) are obtained.

B. Solutions

Equations (10) and (11) are difficult to solve by minimizing the square sum of Eqs. (10) and (11). This is due to the exponential character of the functions in those equations. Hence, we propose a stable method using bracketing [21]. The overview of the algorithm is as follows:

1. First, we select the initial values of T_1' and T_2'. We denote them as t_1' and t_2', respectively.
2. Assuming that t_1' is correct, we solve Eqs. (10) and (11) independently, using bracketing. Let the solutions be t_{2r}' and t_{2g}'.
3. If t_{2r}' and t_{2g}' are sufficiently similar to each other, we output t_1' and $(t_{2r}'+t_{2g}')/2$.
4. Otherwise, we modify t_1' so that the difference between t_{2r}' and t_{2g}' decreases. Again, t_1' can be found using bracketing.
5. Go back to step 2.

In order to realize the above algorithm, we must clarify the following two points:

- How to solve Eqs. (10) and (11).
- How to determine the value of t_1' that decreases the difference between t_{2r}' and t_{2g}', using the bracketing technique.

1. Bracketing for Step 2

The following shows how to solve Eq. (10). The same argument can be applied to Eq. (11). Given an arbitrary T_1', Eq. (10) has a unique solution of T_2' on $T_2'>0$ (under the condition described below.) The solutions can be calculated by bracketing. The initial brackets are automatically determined. They are derived from the shape of the evaluation function Θ_r, which is illustrated in Fig. 2. As the figure shows, Θ_r is convex downward and has only one local minimum. It starts from zero and gradually approaches infinity. Therefore, a solution of T_2' always exists and can be calculated by bracketing. We can randomly select one side of the initial brackets and find the other side by going up or down the slope until the sign of Θ_r changes.

The shape of Θ_* and the conditions for which those equations have solutions are derived from the following propositions:

1. If T_1' is positive, the function Θ_* is convex downward.
2. That $\Theta_*(T_1',0)$ is zero for any T_1'.
3. If T_1' is positive, $\lim_{T_2'\to\infty}\Theta_*(T_1',T_2')=+\infty$.
4. If T_1' is positive, $\Theta_r=0$ has solutions on $T_2'>0$ if and only if

$$i_{r2}\Phi_B(T_1')/\lambda_R - i_{r1}\Phi_R(T_1')/\lambda_B > 0. \tag{16}$$

Similarly, $\Theta_g=0$ has solutions on $T_2'>0$ if and only if

$$i_{g2}\Phi_B(T_1')/\lambda_G - i_{g1}\Phi_G(T_1')/\lambda_B > 0.$$

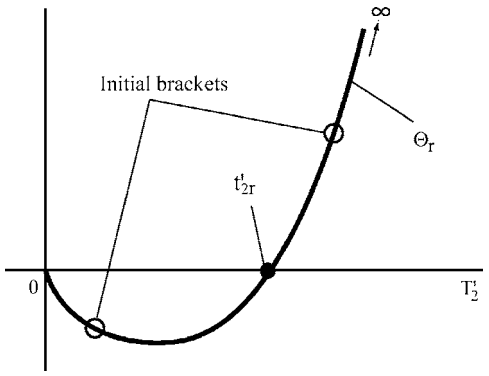

Fig. 2. Shape of the evaluation function Θ_r, given an arbitrary T_1'. A solution of T_2' always exists and can be calculated by bracketing. We let the initial value of t_2' be one side of the brackets and find the other side by going up or down the slope until the sign of Θ_r changes.

Brief proofs of the above propositions are as follows.

Proof of Proposition 1. We show that the second derivative of Θ_r is positive at the extremum D. We used Θ_r for the proof, but the same argument can be done by using Θ_g. We differentiate Θ_r by T_2':

$$\frac{\partial \Theta_r}{\partial T_2'} = \frac{i_{r1}}{\lambda_B}\Phi_R(T_1')\exp(T_2'/\lambda_B) - \frac{i_{r2}}{\lambda_R}\exp(T_2'/\lambda_R)\Phi_B(T_1').$$

From the last equation, T_2', which gives the extremum, can be calculated as

$$T_2' = \frac{\lambda_R\lambda_B}{\lambda_R - \lambda_B}\left(\log\left(\frac{i_{r2}}{\lambda_R}\Phi_B(T_1')\right) - \log\left(\frac{i_{r1}}{\lambda_B}\Phi_R(T_1')\right)\right). \tag{17}$$

According to the Eq. (17), Θ_r has a unique extremum. From the continuity of Θ_r as well as $\partial\Theta_r/\partial T_2', \Theta_r$ is convex upward or convex downward. We further differentiate Θ_r by T_2':

$$\frac{\partial^2 \Theta_r}{\partial T_2'^2} = \left(\frac{1}{\lambda_B} - \frac{1}{\lambda_R}\right)\frac{i_{r1}}{\lambda_B}\Phi_R(T_1')\exp(T_2'/\lambda_B) + \frac{i_{r1}}{\lambda_B}\frac{\partial \Theta_r}{\partial T_2'}.$$

Since $\partial\Theta_r/\partial T_2'$ is zero at the extremum,

$$\frac{\partial^2 \Theta_r}{\partial T_2'^2} = \left(\frac{1}{\lambda_B} - \frac{1}{\lambda_R}\right)\frac{i_{r1}}{\lambda_B}\Phi_R(T_1')\exp(T_2'/\lambda_B).$$

The last equation is positive because $\lambda_B < \lambda_R$. Thus, Θ_r is convex downward. ■

Proposition 2. Trivial. ■

Proposition 3. Trivial. ■

Proof of Proposition 4. We prove only the former part, but the latter can be proved similarly. From Proposition 1, Θ_r is convex downward. That is, the equation possibly has two solutions at most. One of those solutions is zero because of Proposition 2. Consequently, a solution on $T_2' > 0$ exists if the local minimum of Θ_r exists on $T_2' > 0$. Such a condition can be written as Eq. (16) from Eq. (17). A solution on $T_2' > 0$ certainly exists from Proposition 3. ■

2. Bracketing for Step 4

Let us show how to determine a t_1' that decreases the difference between t_{2r}' and t_{2g}'. If t_1' increases/decreases, $t_{2r}' - t_{2g}'$ increases/decreases around the true solution as illustrated in Fig. 3. Therefore, again we can calculate the solutions by bracketing. The facts are derived from the following proposition:

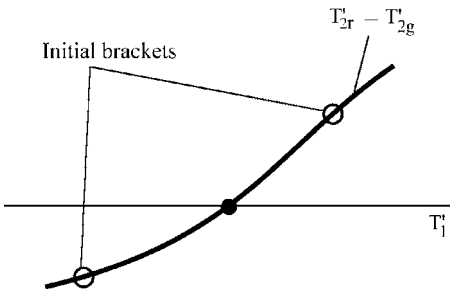

Fig. 3. Shape of $T_{2r}' - T_{2g}'$ around the true solution. If T_1' increases/decreases, $T_{2r}' - T_{2g}'$ increases/decreases. Therefore, the solution can be calculated by bracketing.

5. Let the true solutions be $\hat{T}_1'$ and $\hat{T}_2'$ for Eqs. (10) and (11). If T_1' increases/decreases around them, $T_{2r}' - T_{2g}'$ increases/decreases as long as $\hat{T}_1' > \hat{T}_2'$.

To automatically determine the initial brackets, we need to clarify the shape of the function where it crosses the zero point. The Taylor expansion of Eqs. (10) and (11) is used for this purpose. A detailed derivation of Proposition 5 is as follows:

Derivation of Proposition 5. We derive the Taylor series of Θ_r about a point (t_1', t_{2r}'),

$$\Theta_r = \Theta_r(t_1', t_{2r}') + \left(\frac{i_{r1}\Phi_B(t_{2r}')}{\lambda_R}\exp\left(\frac{t_1'}{\lambda_R}\right) - \frac{i_{r2}\Phi_R(t_{2r}')}{\lambda_B}\exp\left(\frac{t_1'}{\lambda_B}\right)\right)\Delta t_1' + \left(\frac{i_{r1}\Phi_R(t_1')}{\lambda_B}\exp\left(\frac{t_{2r}'}{\lambda_B}\right) - \frac{i_{r2}\Phi_B(t_1')}{\lambda_R}\exp\left(\frac{t_{2r}'}{\lambda_R}\right)\right)\Delta t_{2r}',$$

where $\Delta t_1' = T_1' - t_1', \Delta t_{2r}' = T_{2r}' - t_{2r}'$. We can simplify the last equation using Eq. (10),

$$\Theta_r = i_{r1}\Phi_R(t_1')\Phi_B(t_{2r}')(H_r(t_1')\Delta t_1' - H_r(t_{2r}')\Delta t_{2r}'), \tag{18}$$

where

$$H_r(t) = \frac{\exp(t/\lambda_R)}{\lambda_R\Phi_R(t)} - \frac{\exp(t/\lambda_B)}{\lambda_B\Phi_B(t)}.$$

In a similar way, we derive the Taylor series of Θ_g about another point (t_1', t_{2g}'):

$$\Theta_g = i_{g1}\Phi_G(t_1')\Phi_B(t_{2g}')(H_g(t_1')\Delta t_1' - H_g(t_{2g}')\Delta t_{2g}'). \tag{19}$$

From the last two equations, $T_{2r}' - T_{2g}'$ against $\Delta t_1'$ can be expressed as

$$T_{2r}' - T_{2g}' = \left(\frac{H_r(t_1')}{H_r(t_{2r}')} - \frac{H_g(t_1')}{H_g(t_{2g}')}\right)\Delta t_1' + (t_{2r}' - t_{2g}').$$

Around the true solutions $\hat{T}_1', \hat{T}_2'$, the last equation becomes

$$T_{2r}' - T_{2g}' = \left(\frac{H_r(\hat{T}_1')}{H_r(\hat{T}_2')} - \frac{H_g(\hat{T}_1')}{H_g(\hat{T}_2')}\right)\Delta t_1'. \tag{20}$$

The following function

$$I(T_1', T_2') = H_r(T_1')H_g(T_2') - H_g(T_1')H_r(T_2') \tag{21}$$

is obviously $I(T_1', T_2') = -I(T_2', T_1')$. We confirmed that $I(T_1', T_2')$ is positive if T_1' is larger than T_2' by calculating every case from 2000 to 10,000 K with a 1 K interval.

4. EXPERIMENTS AND RESULTS

A. Evaluating Effectiveness Using Simulation Data

The effectiveness of the proposed method is evaluated with simulation data. In particular, we checked the following two points: (1) average estimation error using simulation data and (2) dependency on initial values.

The error was defined as the difference between estimated and true reciprocal color temperatures. Reciprocal

color temperatures were proposed by Judd [22], in which differences correspond more closely to equal perceptual color differences than to normal color temperatures. The unit is called "mired" ($=10^6\,\mathrm{K}^{-1}$) and is defined as $T^{\mathrm{rec}}=10^6/T$. Empirically, the just noticeably different (JND) chromaticity difference is 5.5 mired [11,22]. The range from 2500 to 8500 K in color temperatures corresponds to the range from 400 to 118 mired in reciprocal color temperatures.

1. Estimation Error with Simulation Data

Methods. We calculated the average estimation error using seven kinds of blackbody illuminants and six kinds of reflectance. The total combination was ${}_7C_2\times 6=126$. A camera sensitivity, which is 1 at a particular wavelength (red, 624 nm; green, 548 nm; blue, 480 nm) and is 0 at others was used. The seven color temperatures were 2500 K, 3500 K, 4500 K, 5500 K, 6500 K, 7500 K, and 10,000 K. The six reflectance patches were "Red," "Blue," "Green," "Cyan," "Magenta," and "Yellow" in the GretagMacbeth ColorChecker, hereafter referred to as "Macbeth." All the reflectance data were obtained by measuring the spectrum of a color patch with a spectrometer (Photo Research PR-650) under a known illuminant.

Results. The average estimation error was 1.64×10^{-5} mired for T_1 and 1.74×10^{-5} mired for T_2, as shown in Table 1. The estimation by the previous method [16] is also shown for reference. The error converges to zero in all cases by using the proposed method.

2. Dependency on Initial Values

Methods. We did our estimation 500 times with different initial values but with the same reflectance and illuminants and calculated the average and the standard deviation of the estimation error. A camera sensitivity that is 1 at the wavelength (red, 624 nm; green, 548 nm; blue, 480 nm) and is 0 at others was used. The color temperatures of illuminants were 3500 and 7500 K. We used "red" reflectance of the Macbeth ColorChecker. Initial values were randomly and uniformly distributed over the range of the true temperature ±1000 K.

Results. The averages and the standard deviations of the estimation error were 3.53×10^{-6} mired and 2.18×10^{-6} mired for T_1, and 3.78×10^{-6} mired and 2.35×10^{-6} mired for T_2, as shown in Table 2. The standard deviation is nearly the estimation accuracy, which is about 10^{-6} due to the machine accuracy. Therefore, we conclude that initial values do not affect the estimation. However, the result temperatures can be an impractical number, such as 2×10^{12} K if the relation (for instance, $T_1>T_2$) is reversed in the initial values ($T_1<T_2$). In other words, initial values can be any numbers if the relation between T_1 and T_2 is retained.

Table 1. Average Estimation Error in 126 Experiments Using Simulation Data[a]

Method	T_1 Error (mired)	T_2 Error (mired)
Proposed method	1.64×10^{-5}	1.74×10^{-5}
Previous method	5.11×10	5.52×10

[a]The estimation error by the previous method [16] is also shown for reference.

Table 2. Average and Standard Deviation of Estimation Errors in 500 Experiments with Different Initial Values

Parameter	T_1 Error (mired)	T_2 Error (mired)
Average	3.53×10^{-6}	3.78×10^{-6}
Standard deviation	2.18×10^{-6}	2.35×10^{-6}

B. Applying the Algorithm to Real Data

We conducted four sets of experiments to see whether the method could work on real data. In the first set of experiments, we tested our algorithm with various kinds of natural illuminants and reflectances, and erroneous results were obtained. Therefore, we presumed there are two causes of the error. One cause might have been the failure of the blackbody radiation to accurately portray the actual illuminants. To understand this problem, we conducted the second set of experiments and observed how the violation of the blackbody assumption affects the estimation. We also tested how different real spectra appear to blackbody radiations in the third set of experiments. The other cause of error must have been the violation of the narrowband sensitivity assumption. We tested how it affects the estimation in the fourth set of experiments.

The following explains experiments that were conducted, and each focuses on: (1) estimation error on experiments with real data, (2) error caused by the assumption of blackbody illumination, (3) difference between spectra of the blackbody radiation and real spectra, and (4) error caused by the assumption of narrowband sensitivity.

1. Estimation Error with Real Data

Methods. We calculated the average estimation error using eight kinds of natural illuminants and six kinds of reflectance. The total combination was ${}_8C_2\times 6=168$. The sensitivity of bandpass filters (MellesGriot 03FIV119, 03FIV111, 03FIV004) was used for the camera sensitivity. Their full width at half-maximum was 10 nm, and their center wavelengths were as follows: red, 620 nm; green, 532 nm; and blue, 450 nm. They are shown as "Filter" in Fig. 4. Eight illuminants were A, B, C of CIE standard illuminants and Judd daylight phases D48, D55, D65, D75, and D100 [19]. The six reflectances were "Red," "Blue," "Green," "Cyan," "Magenta," and "Yellow" of Macbeth.

Results. The average estimation error was 3.67×10^{3} mired for T_1, and 1.17×10^{4} mired for T_2, as shown in Table 3. The erroneous results force us to think what the substantial causes of those errors are. As stated in the beginning of this subsection, there are two possible causes: the violations of the blackbody assumption and the narrowband sensitivity assumption. The following experiments investigated how the violations affect the estimation. We discuss the robustness of the method in Section 5.

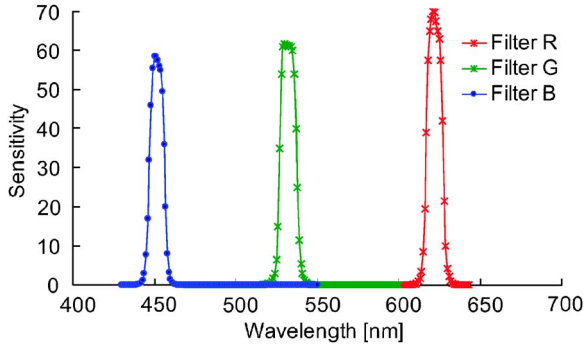

Fig. 4. (Color online) Camera sensitivities used in the first experiments in Subsection 4.B. They are the sensitivities of bandpass filters (MellesGriot 03FIV119, 03FIV111, 03FIV004).

Table 3. Average Estimation Error in 168 Experiments Using Real Data[a]

Method	T_1 Error (mired)	T_2 Error (mired)
Proposed method	3.67×10^3	1.17×10^4
Previous method	7.97×10	8.43×10

[a]The estimation error by the previous method [16] is also shown for reference.

2. Error Caused by the Blackbody Assumption

Methods. We plotted the change of the estimation error against the error on illumination chromaticity. Let Δe_r and Δe_g be the error on illumination chromaticity. One illumination chromaticity was chosen, and Δe_r and Δe_g were added to it. Δe_r and Δe_g were changed from 0 to 1% by 0.1%. Camera sensitivity is 1 at these wavelengths (red, 624 nm; green, 548 nm; blue, 480 nm) and is 0 at others. The color temperatures were 3000 and 9000 K. The reflectance was "dark skin," i.e., the top-left brown reflectance of the Macbeth ColorChecker.

Results. The ΔT1 and ΔT2 in Fig. 5 show the estimation error ΔT_1 and $\Delta T2$ against the percentage of the modeling error Δe_r and Δe_g of illumination colors. The unit of the horizontal axis is percent, and that of the vertical axis is mired. Figure 5 also shows the line of JND chromaticity difference (5.5 mired). The figure shows that the modeling error should be under about 0.1% if we want the estimation error to be lower than 5.5 mired.

3. Difference between Blackbody and Real Spectra

Methods. We calculated the difference between blackbody illuminants and real illuminants. First, we searched for the blackbody color temperature whose color is the nearest to that of the real illuminant. Then we calculated the color difference between the two. The value that represents the difference is defined as (chromaticity of the real illuminant − chromaticity of the searched color temperature)/(chromaticity of the searched color temperature). Spectra of the CIE standard illuminants (A,B,C) and Judd's daylight phases (D48, D55, D65, D75, D100) were used for the calculation. A sensitivity that is 1 at 620 nm (red), 532 nm (green), 450 nm (blue) and 0 at others was used.

Results. Table 4 shows the difference between the color of blackbody and real spectra, Except for CIE standard illumination A, all illumination has more than a 0.1% difference. Therefore, the proposed method would produce significant errors when those illuminants were used.

4. Error Caused by the Narrowband Assumption

Method. We made a virtual sensitivity with variable bandwidth by using the Gaussian function. The σ of the Gaussian function was the parameter to change the bandwidth. The center wavelengths were as follows: red, 620 nm; green, 532 nm; and blue, 450 nm. Two examples of those sensitivities are shown in Fig. 6. One with σ

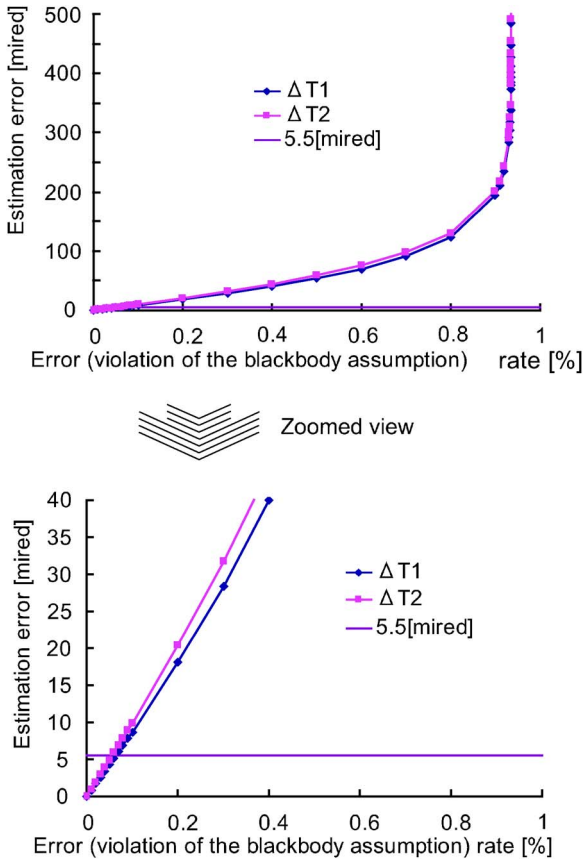

Fig. 5. (Color online) Plots of the estimation error against the violation of the blackbody assumption; "ΔT1" and "ΔT2" express the estimation error. JND chromaticity difference (5.5 mired) is also shown. To limit the estimation error to lower than 5.5 mired, the violation should be under about 0.1%.

Table 4. Difference between Blackbody and Real Spectra[a]

Illuminants	Δe_r (%)	Δe_g (%)	Nearest T (K)
CIE A	0.0029	−0.0165	2856
CIE B	2.6368	−4.6126	5087
CIE C	5.5397	−6.1154	7451
Judd D48	−1.0788	2.0506	4818
Judd D55	−1.0617	1.6286	5584
Judd D65	−0.9358	1.1519	6698
Judd D75	−0.7690	0.8096	7842
Judd D100	−0.4606	0.3816	10852

[a]We searched for the blackbody that has the color nearest to that of the real spectrum and calculated the chromaticity difference between the two. Note that the difference is defined in the color space of the sensitivity used in this experiment.

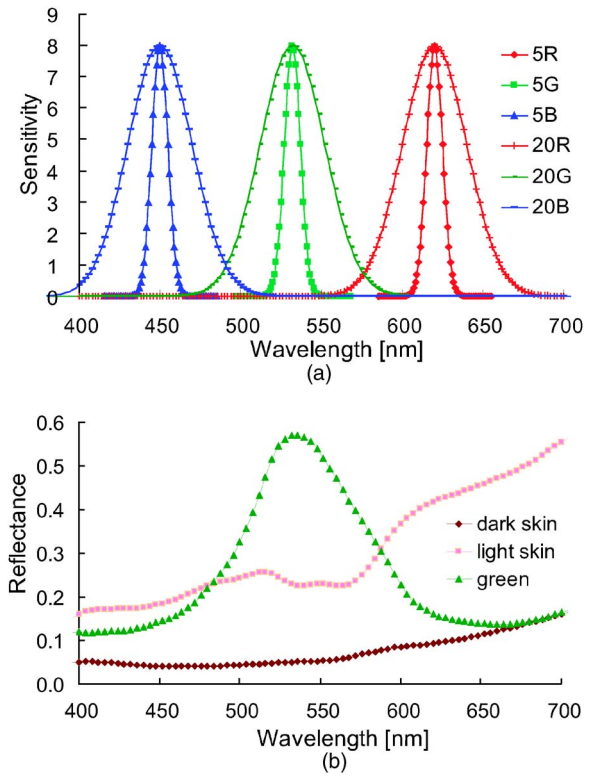

Fig. 6. (Color online) Data used in the fourth experiments in Subsection 4.B. (a) Virtual camera sensitivities. Here "5" and "20" are Gaussian functions whose standard deviation is 5 and 20 nm, respectively. (b) Reflectances. Three reflectances are "dark skin," "light skin," and "Green" of the Macbeth ColorChecker. "Dark skin" varies linearly around wavelengths of a camera sensitivity compared with "green" and "light skin."

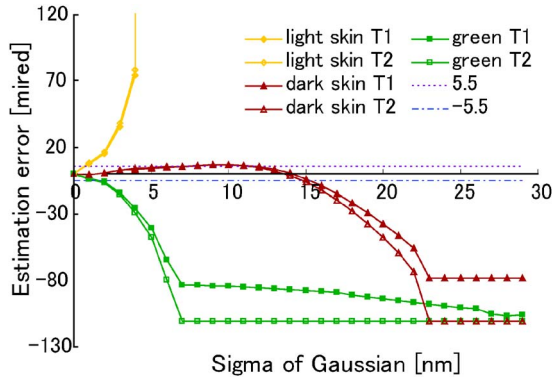

Fig. 7. (Color online) Plot of the estimation error against the violation of the narrowband sensitivity assumption. The more the bandwidth of a camera sensitivity (the standard deviation σ of a Gaussian function) grows, the larger the estimation error becomes. Three reflectances, "dark skin," "light skin," and "green" were tested. The speed of the error growth depends on the reflectance.

$=5$ nm is shown as "5," and $\sigma=20$ nm is shown as "20." Color temperatures of illuminants were 4000 K and 9000 K. We used "dark skin," "light skin," and "Green" of Macbeth for the reflectance. Figure 6 shows them denoted by "dark skin," "light skin," and "green," respectively.

Results. Figure 7 shows the estimation error against the bandwidth of a camera's sensitivity. The more the bandwidth (the standard deviation σ of a Gaussian function) grows, the larger the estimation error becomes. The speed of the error growth depends on the reflectance. In the case of "green" or "light skin" reflectance, the estimation breaks down when the σ of the Gaussian function is larger than 5 nm, while in the case of "dark skin," the estimation performs well until the a becomes 20 nm. If a reflectance varies linearly around wavelengths of a camera's sensitivity, the integration in Eq. (3) becomes a multiplication by a constant number. Then the modeling error by the narrowband assumption can be ignored. Otherwise, the modeling error affects the estimation. As Fig. 6 shows, the reflectance "dark skin" varies linearly around wavelengths of a camera's sensitivity compared with "green" and "light skin." When σ is set to 5 nm, half of the test data set provided good results within the error of 5.5 mired.

5. DISCUSSION

Assuming illumination to be the blackbody radiation made the estimation sensitive to the modeling error. There are two other ways to express illumination by a one-dimensional parameter. One is to use Wien's approximation for blackbody radiation, and the other is to use the straight-line approximation of Finlayson *et al.* The blackbody illumination model can be compared with those models. Wien's approximation to the Planck formula can be expressed as

$$M(\lambda,T) \simeq c_1\lambda^{-5}\exp(c_2/\lambda T)^{-1}. \tag{22}$$

From the last equation, we can derive the following relation [12,20]:

$$e_r = me_g^A, \tag{23}$$

where $\vec{e}=[e_r,e_g]^t$ is an illumination chromaticity, $A=(1/\lambda R-1/\lambda B)/(1/\lambda G-1/\lambda B)$ and $m=\lambda_G^{5A}/(\lambda_R^A\lambda_B^{5A-5})$ are constant numbers characterizing a camera. If we substitute the equation into Eqs. (12) and (13), we obtain two redundant equations and cannot determine the solutions for each color temperature. The Planck formula and Wien's approximation are very similar when the color temperature is low. Therefore, estimation of our method would be unstable if the two color temperatures of input illumination are both low.

Finlayson *et al.* assumed that natural daylight illumination falls on a line [16] in an inverse-chromaticity space. Namely, they assumed the following relation:

$$1/e_g = m(1/e_r) + c. \tag{24}$$

Note that the last equation does not appear in Ref. [16], but it expresses its idea. Reference [16] assumes that a set of all diagonal matrices mapping chromaticities under arbitrary illumination (e_r,e_g) to canonical illumination $(e_r^{\text{canonical}},e_g^{\text{canonical}})$ appears linear in the 1st–2nd diagonal matrix component space. In other words, it assumes $f(x)=m'x+c'$, where x and $f(x)$ correspond to the first and the second diagonal matrix components $e_r^{\text{canonical}}/e_r$ and $e_g^{\text{canonical}}/e_g$, respectively. We can derive Eq. (24); since both $e_r^{\text{canonical}}$ and $e_g^{\text{canonical}}$ could be any constant numbers, they can be replaced by (1, 1).

Table 5. Difference between Real Illumination Colors and Colors Calculated from the Straight-Line Illumination Model

Illuminants	Δe_r (%)	Δe_g (%)
CIE A	6.9829	−7.2289
CIE B	−1.9758	4.0070
CIE C	−1.1578	2.7347
Judd D48	−0.6929	1.3720
Judd D55	−0.4382	0.9421
Judd D65	−0.0239	0.0553
Judd D75	0.3781	−0.9191
Judd D100	1.0385	−2.6985

If we substitute the last equation into Eqs. (12) and (13), we can solve all the unknown parameters explicitly. (This paper was inspired by this discovery.) The gradient m and the intercept c in Eq. (24) are constant numbers calculated by least-square fitting to the data of CIE standards and Judd's daylight phases. The difference between those illumination data points and the straight line is shown in Table 5. Considering the results shown in Table 3, the previous method, the straight-line model of Finlayson *et al.*, is the most successful, and we think that this is the only model for solving color constancy with illumination constraint. However, as shown in Tables 3 and 5, even the straight-line model cannot help suffering from the effect of the modeling error.

Thus, the comparison of one-dimensional models of the illumination shows that illumination color constraint can work by itself as long as there is no modeling error. However, the modeling error cannot be ignored and must be considered in order to perform stable and accurate color constancy. We conclude that both illumination constraint and other rich information, such as assumptions on reflectances, should be taken into account for a robust estimation.

6. CONCLUSION

We proposed what we believe to be a new method to solve the color constancy problem by exploiting blackbody radiation. Based on the approach, we examined and obtained the results in the following four areas: (1) Our method performed considerably well in the experiments with simulation data. (2) To achieve the accuracy within the error of just noticeable differences (JND), the modeling error between the blackbody radiation and the illuminants should be lower than 0.1%. (3) Although the method uses initial values, the results do not depend on how to choose them. (4) Most illuminants differ from the blackbody radiation by more than 0.1%. The discussion about the robustness of our method and the possibility of solving color constancy using a one-dimensional model of the illumination shows that much information, such as assumptions about reflectances, should be taken into account with the constraint on illumination to achieve stable and accurate color constancy.

ACKNOWLEDGMENT

This research was supported in part by the Ministry of Education, Culture, Sports, Science and Technology under the Leading Project, "Development of High Fidelity Digitization Software for Large-Scale and Intangible Cultural Assets."

REFERENCES

1. M. D'Zmura and P. Lennie, "Mechanisms of color constancy," J. Opt. Soc. Am. A **3**, 1662–1672 (1986).
2. H. C. Lee, "Method for computing the scene-illuminant from specular highlights," J. Opt. Soc. Am. A **3**, 1694–1699 (1986).
3. S. Tominaga and B. A. Wandel, "Standard surface-reflectance model and illuminant estimation," J. Opt. Soc. Am. A **6**, 576–584 (1989).
4. H. C. Lee, "Illuminant color from shading," Proc. SPIE **1250**, 233–244 (1990).
5. B. V. Funt, M. Drew, and J. Ho, "Color constancy from mutual reflection," Int. J. Comput. Vis. **6**, 5–24 (1991).
6. G. D. Finlayson and G. Schaefer, "Solving for color constancy using a constrained dichromatic reflection model," Int. J. Comput. Vis. **42**, 127–144 (2001).
7. R. T. Tan, K. Nishino, and K. Ikeuchi, "Color constancy through inverse intensity-chromaticity space," J. Opt. Soc. Am. A **21**, 321–334 (2004).
8. D. H. Brainard and W. T. Freeman, "Bayesian color constancy," J. Opt. Soc. Am. A **14**, 1393–1411 (1997).
9. G. D. Finlayson, S. D. Hordley, and P. M. Hubel, "Color by correlation: a simple, unifying, framework for color constancy," IEEE Trans. Pattern Anal. Mach. Intell. **23**, 1209–1221 (2001).
10. S. Tominaga, S. Ebisui, and B. A. Wandell, "Scene illuminant classification: brighter is better," J. Opt. Soc. Am. A **18**, 55–64 (2001).
11. S. Tominaga and B. A. Wandell, "Natural scene-illuminant estimation using the sensor correlation," Proc. IEEE **90**, 42–56 (2002).
12. G. D. Finlayson and S. D. Hordley, "Color constancy at a pixel," J. Opt. Soc. Am. A **18**, 253–264 (2001).
13. J. M. Geusebroek, R. Boomgaard, S. Smeulders, and T. Gevers, "*A physical basis for color constancy*," *in Proceedings of the First European Conference on Colour in Graphics, Image and Vision* (CGIV, 2002), pp. 3–6.
14. M. D'Zmura, "Color constancy: surface color from changing illumination," J. Opt. Soc. Am. A **9**, 490–493 (1992).
15. Y. Ohta and Y. Hayashi, "Recovery of illuminant and surface colors from images based on the CIE daylight," in *Proceedings of the Third European Conference on Computer Vision* (CGIV, 1994), Vol. II, pp. 235–246.
16. G. D. Finlayson, B. V. Funt, and K. Barnard, "Color constancy under varying illumination," in *Proceedings of IEEE International Conference on Computer Vision* (IEEE, 1995), pp. 720–725.
17. K. Barnard, G. Finlayson, and B. Funt, "Color constancy for scenes with varying illumination," Comput. Vis. Image Underst. **65**, 311–321 (1997).
18. E. H. Land and J. J. McCann, "Lightness and retinex theory," J. Opt. Soc. Am. **61**, 1–11 (1971).
19. D. B. Judd, D. L. MacAdam, and G. Wyszecky, "Spectral distribution of typical daylight as a function of correlated color temperature," J. Opt. Soc. Am. **54**, 1031–1040 (1964).
20. J. A. Marchant and C. M. Onyango, "Shadow-invariant classification for scenes illuminated by daylight," J. Opt. Soc. Am. A **17**, 1952–1961 (2000).
21. W. H. Press, B. P. Flannery, S. A. Teukolsky, and W. T. Vetterling, *Numerical Recipes in C* (Cambridge U. Press, 1988).
22. D. B. Judd, "Sensibility to color-temperature change as a function of temperature," J. Opt. Soc. Am. **23**, 127–134 (1933).